

Superfluid flow past an obstacle in annular Bose–Einstein condensates

M Syafwan¹, P Kevrekidis², A Paris-Mandoki³, I Lesanovsky³,
P Krüger³, L Hackermüller³ and H Susanto⁴

¹Department of Mathematics, Andalas University, Limau Manis, Padang, 25163, Indonesia

²Department of Mathematics and Statistics, University of Massachusetts, Amherst, MA 01003-9305

³School of Physics and Astronomy, University of Nottingham, Nottingham, NG7 2RD, United Kingdom

⁴Department of Mathematical Sciences, University of Essex, Colchester, CO4 3SQ, United Kingdom

E-mail: hsusanto@essex.ac.uk, lucia.hackermuller@nottingham.ac.uk

Abstract. We investigate the flow of a one-dimensional nonlinear Schrödinger model with periodic boundary conditions past an obstacle, motivated by recent experiments with Bose–Einstein condensates in ring traps. Above certain rotation velocities, localized solutions with a nontrivial phase profile appear. In striking difference from the infinite domain, in this case there are many critical velocities. At each critical velocity, the steady flow solutions disappear in a saddle-center bifurcation. These interconnected branches of the bifurcation diagram lead to additions of circulation quanta to the phase of the associated solution. This, in turn, relates to the manifestation of persistent current in numerous recent experimental and theoretical works, the connections to which we touch upon. The complex dynamics of the identified waveforms and the instability of unstable solution branches are demonstrated in 1D simulations. Proof-of-principle 2D simulations corroborating the emergence of persistent current in the latter setting are also performed.

PACS numbers: 03.75.Kk, 67.85.-d, 37.10.Vz, 47.37.+q

1. Introduction

Persistent flow is a remarkable property of macroscopic quantum systems. Bose–Einstein condensates (BECs) in a ring geometry [1, 2, 3, 4, 5] have been shown recently to support circulating superfluid flow [6, 7, 8]. The ring trap can have a highly tunable radius and controllable transverse oscillation frequency [9, 10], which makes such a system ideal for the creation of, e.g., a multiply connected BEC [8] as well as for applications in interferometry [11].

A characteristic feature associated with superfluidity is the existence of a critical velocity above which its breakdown leads to the creation of excitations. In experiments with BECs, evidence for a critical velocity was obtained by moving an obstacle, i.e. a tightly focused laser beam, through a BEC [12, 13]. This setting has been demonstrated to be prototypical for dark soliton formation in 1D [14, 15] (see [16] for experiments, although the latter were only quasi-one-dimensional), and for vortex formation in 2D [17], which can be thought of as a type of nonlinear Cherenkov radiation. In the case of obstacles in a supersonic flow of the BEC, the formed Cherenkov cone [18, 19] transforms into a spatial shock wave consisting of a chain of dark solitons [20]. The appearance of such radiation in photonic crystals [21] is yet another illustration of the importance of the fundamental study of critical velocity. The formation of vortex dipoles in a similar setting was also directly observed experimentally in the work of [22].

In a homogeneous weakly interacting Bose gas the critical velocity is the same as the speed of sound, as per the associated Landau criterion [23]. Moving inhomogeneities can alter this critical value. For a ring geometry it has been shown in [24] that the instability of the superfluid is caused by outer and inner edge surface modes, in a similar fashion as in an infinite cylindrically symmetric tube with transverse harmonic confinement [25, 26]. The different mechanism is due to the presence of a centrifugal force arising from the nature of the rotation. The effect of potential barriers in BECs confined in a ring trap has been studied experimentally and theoretically [7, 27, 28, 29]. The weak link due to the barrier, which affects the current around the loop, has a promising application as a closed-loop atomic circuit (atomtronics), e.g. as analogs of superconducting quantum interference devices (SQUIDs) [30, 31]. The existence of a critical velocity above which superfluid flow stops in the ring is connected to Cherenkov radiation through the excitations of vortex-antivortex pairs [7, 27], in analogy to the rectilinear case [22]. Nevertheless, the relevant instability remains somewhat inconclusive (in connection to corresponding experiments [7]) with different mechanisms proposed to account for discrepancies between theory and observation including thermal fluctuations [32] and imaging system resolution [33].

In the present study we consider a BEC confined in an effectively one- and also in a two-dimensional annular trap with a moving potential barrier, which is equivalent to a stationary barrier and a moving condensate as realized in [7, 28]. Using the mean-field, i.e. Gross-Pitaevskii (GP) approximation in the *infinite* domain, it was shown that the critical velocity v_c corresponds to a saddle-center bifurcation of two branches of solutions

[14], a stable (center) and an unstable (saddle) one. Using a 1D approximation (for a narrow ring geometry) in an effectively periodic domain, we reveal in an analytical and corroborate in a numerical fashion the existence of a sequence of saddle-center bifurcations and associated critical velocities. These, in turn, correspond to different topological charges that are all connected within the same bifurcation diagram. We present numerical simulations as well as analytical calculations, where it is shown that the critical points can be obtained from solving two coupled nonlinear equations. We also observe the presence of a critical strength of the inhomogeneity (or length of the domain) above (respectively, below) which there is no critical velocity, i.e. the inhomogeneity can move with any velocity while preserving the superfluidity. This occurs when the ring circumference becomes shorter than the healing length (a setting that may thus be less relevant from a physical perspective) or when the obstacle is strong enough. Our examination reveals a series of unstable branches in the relevant dynamics; we explore the dynamical evolution of the solutions associated with these branches by means of direct numerical simulations. We show that the relevant phenomenology is robust and persists in higher dimensions. To illustrate this, we consider the case of a two-dimensional annular stripe domain.

The results presented here are intimately connected with recent experimental and theoretical observations. One of the early attempts to identify topological winding (and unwinding) in atomic BECs resulted in the seminal findings of [34, 35, 36]. In these works, rather than a defect rotating inside a BEC, a setting where a rotation was imposed on the entire quasi-1D ring BEC was examined. This has similarities but also substantial differences from our setup. A similarity is that the system is analytically tractable; in fact, it is a genuinely homogeneous system (1D in the co-rotating frame) where the effective 1D GP equation associated with the dynamics (including the rotational term) can be solved analytically by means of elliptic function cnoidal wave solutions which account for the phase slip events also identified here. On the other hand, there are nontrivial differences from that case. In particular, in our setting (and in recent experiments such as [7, 28, 29, 30, 31, 37], the phase slips do not arise in a “distributed” manner, associated with these periodic cnoidal solutions, but rather in a localized manner being co-located with the defect. Hence, the analytical considerations presented herein are expected to be more closely connected to recent experiments. Among the latter, a few [30, 31] have been more directly related to the case with a pair of weak links or Josephson junctions, aiming at least in part to potential superconducting quantum interference (SQUID) related applications, while here we will focus solely on the realm of a single weak link. Arguably, the recent experimental settings most clearly related to our own work are those of [28, 29]. The former one measures experimentally the emergence of the phase slips and uses a qualitative model based on the Bohr-Sommerfeld quantization condition and an approximate current-phase relation at the weak link to theoretically trace a structure similar to the one that we analytically identify in the present work [cf. their Fig. 4 and our bifurcation diagrams of Figs. 2 and 3 below]. The latter work of [29], in fact, explicitly identifies the hysteretic dynamics

that has been proposed to be a key characteristic of this system in the above figures. However, it also recognizes the disparity of the experimental observations from the Gross-Pitaevskii findings (a feature that retraces discussions of earlier work mentioned above [32, 33]). The analytical tractability of our findings in this system (in a sense, adapting to it the spirit of calculations performed earlier in the homogeneous rotated system of [34, 35, 36]) may offer further insight in the relevant comparison.

As a final step in this theme of comparisons, we would like to mention recent work, which has explored the case of a rotating weak link as a function not of the potential/domain parameters considered here (such as the barrier strength or the domain length), but rather as a function of the interaction strength [38]. This elaborate task requires different approaches in the weakly interacting limit (treated by means of a Gross-Pitaevskii equation) and in the strongly interacting limit (treated by means of a Luttinger liquid approach and in the case of a Tonks gas by a Bose-Fermi mapping to the case of non-interacting fermions). Intermediate regimes were treated by density-matrix renormalization group computations which, in fact, revealed an unexpected optimality in the observed persistent currents at some intermediate interaction strengths between the above limits.

2. Theoretical Setup

We consider a BEC in a ring trap with a moving obstacle. The setup is described by the 2D GP equation [39, 40]

$$i\hbar\partial_t\psi = -\frac{\hbar^2}{2m}\Delta\psi - \mu\psi + g_{2D}|\psi|^2\psi + U(r, \theta, t)\psi, \quad (1)$$

where $\psi(r, \theta, t)$ is the mean-field wave function, m is the atomic mass, $\Delta = \partial_{rr} + \partial_r/r + \partial_{\theta\theta}/r^2$ is the Laplacian in polar coordinates ($r \in [R_o, R_i], \theta \in [0, 2\pi]$), μ is the chemical potential, $g_{2D} = g/(\sqrt{2\pi}l_z)$, $g = \frac{4n\pi\hbar^2 a}{m}$ the atomic interaction strength, which in 3D is proportional to the atomic scattering length a , n ($\sim 10^3 - 10^7$) is the number of atoms, $l_z = \sqrt{\hbar/m\omega_z}$ is the transverse harmonic oscillator length, ω_z is the longitudinal trap frequency, and U is a short range potential moving with an angular velocity ω . This potential can be treated as a δ potential of strength α , i.e., $U(r, \theta, t) = \alpha\delta(r - L/\pi)\delta(\theta - \omega t)$. We assume that the annular trapping potential centred at $L/\pi = (R_o + R_i)/2$ behaves in a way such that it can be effectively represented by the homogeneous Dirichlet boundary conditions $\psi(R_o, \theta, t) = \psi(R_i, \theta, t) = 0$. For a general discussion independent of the chosen atomic system, we will express Eq. (1) in a dimensionless form, which can be achieved by using $\Lambda = mg_{2D}/\hbar^2$, $\Omega = \hbar/m\Lambda^2$ and setting $r = \Lambda\tilde{r}/\sqrt{2}$, $t = \tilde{t}/\Omega$, $\psi = \tilde{\psi}/\Lambda^{3/2}$.

First, we consider the case with $(R_o - R_i) \ll 1$, e.g. a quasi 1D situation, in which case in a frame rotating with angular velocity v , Eq. (1) can be reduced into the scaled equation

$$i\partial_t\psi = -\partial_{xx}\psi - \mu\psi + |\psi|^2\psi + \alpha\delta(x - vt)\psi, \quad (2)$$

where $-L \leq x = \theta \frac{L}{\pi} - L < L$ and the periodic boundary conditions along the azimuthal direction are

$$\psi(-L, t) = \psi(L, t), \quad \partial_x \psi(-L, t) = \partial_x \psi(L, t). \quad (3)$$

In a second step we extend our findings to 2D by considering the original setup (1) with the potential U in the shape of an annular disk rotating with velocity v , i.e.,

$$U(x, y) = \begin{cases} \tilde{\alpha}, & (x - x_0)^2 + (y - y_0)^2 < 1/4, \\ 0, & \text{elsewhere,} \end{cases}$$

where $x_0 = \frac{1}{2}(R_o + R_i) \cos(vt)$ and $y_0 = \frac{1}{2}(R_o + R_i) \sin(vt)$.

A static BEC with a moving potential is equivalent to the flow of a nonlinear Schrödinger (NLS) fluid past an immobile obstacle. Therefore, considering the travelling frame (i.e., $x \rightarrow x - vt$), Eq. (2) for the effectively 1D problem can be written as

$$i\partial_t \psi = iv\partial_x \psi - \partial_{xx} \psi - \mu\psi + |\psi|^2 \psi + \alpha\delta(x)\psi. \quad (4)$$

In order to study the existence of persistent superflow, we search for a steady state solution $\psi(x, t) = u(x)$ of the GP equation (4). The time-independent version of (4) is solved simultaneously with the scaling equation $\int_{-L}^L |u|^2 dx = N$, where without loss of generality we choose $N = 2L$, using a Newton-Raphson method by discretizing the Laplacian with a central finite difference method [41].

We then examine the (linear) stability of a solution $u(x)$ for which we introduce the linearization ansatz $\psi(x, t) = u(x) + \epsilon(r(x)e^{i\omega t} + s^*(x)e^{-i\omega^* t})$, where ϵ is a formal small parameter, ω an eigenfrequency and (r, s) an eigenvector. Substituting it into eq. (4) and keeping the linear terms in r and s , one obtains the linear eigenvalue problem (EVP)

$$\begin{bmatrix} \mathcal{L} & u^2 \\ -(u^*)^2 & -\mathcal{L}^* \end{bmatrix} \begin{bmatrix} r(x) \\ s(x) \end{bmatrix} = -\omega \begin{bmatrix} r(x) \\ s(x) \end{bmatrix}, \quad (5)$$

where $\mathcal{L} = iv\partial_x - \partial_{xx} + 2|u|^2 - \mu + \alpha\delta(x)$. A solution $u(x)$ is stable if and only if $\text{Im}(\omega) = 0$ for all eigenfrequencies ω .

3. Numerical Results and Connections to Theory

In Figure 1 we show one of the principal results of the present work, namely the bifurcation diagram of superfluid flow for varying velocity v starting from the static solution $v = 0$ of (2) for a system with $N = 2L = 10$ and $\alpha = 0.5$. As we fix the norm, the bifurcation diagram is depicted in μ as a function of v . From Figure 1 we observe that the solution experiences many saddle-center bifurcations (turning points) as indicated by black dots. Since steady flows do not exist beyond the turning points (i.e. for either larger or smaller v for the respective turning point), the abscissa of the bifurcation points corresponds to critical velocities v_c .

In a ring trap geometry the phase of the BEC circulates around the centre by an integer multiple of 2π (see figure 1). The so-called topological charge q corresponds to how many times the phase winds along the ring. Macroscopic states with different q

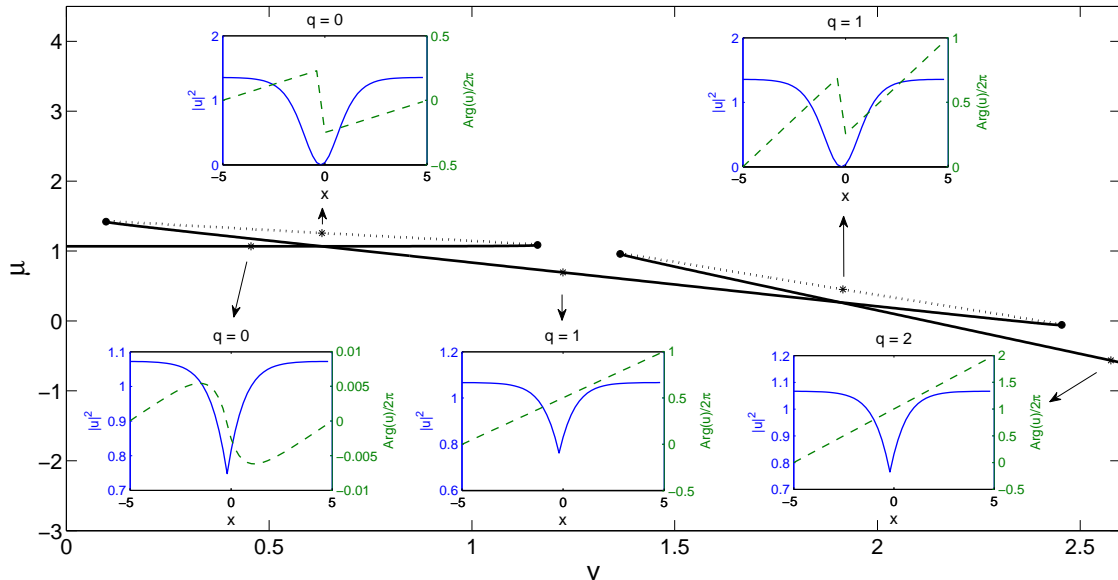


Figure 1. Bifurcation diagram of the steady flow solution for a model system with $\alpha = 0.5$ and $N = 2L = 10$. Bold solid and dotted lines correspond to stable and unstable solutions, respectively. The insets show the time independent solution profiles in the ring trap along the branches for velocities corresponding to the position of the crosses. Solid and dashed lines in the insets show the magnitude and phase of the solutions. For each profile the solution charge q is given.

have distinct energies and the effect of q on persistent flow has been recently studied experimentally [8]. Considering the phase of the solutions along the branch in figure 1, it is interesting to note that the topological charge jumps along the branch segments that correspond to decreasing velocity v . More precisely, q increases at the points where the density at the obstacle vanishes. Hence, the solutions for all values of q are smoothly connected along the diagram. In Fig. 1, the upper insets show the density and the phase profile right before the charge jump (phase slip).

To provide a better understanding of the relation between the bifurcation diagram in ring systems (figure 1) and that of the infinite domain, which only has one saddle-center bifurcation [14], we now study bifurcation diagrams for different values of the domain length L . For this calculation it is preferable to fix the chemical potential μ and let the solution norm vary. Using $\alpha = 0.5$ and $\mu = 1$, the results are shown in Fig. 2. Plotted is the density of the stationary solution $|u(0)|^2$ against the velocity.

It is known that in the infinite domain, the critical velocity corresponds to a saddle-

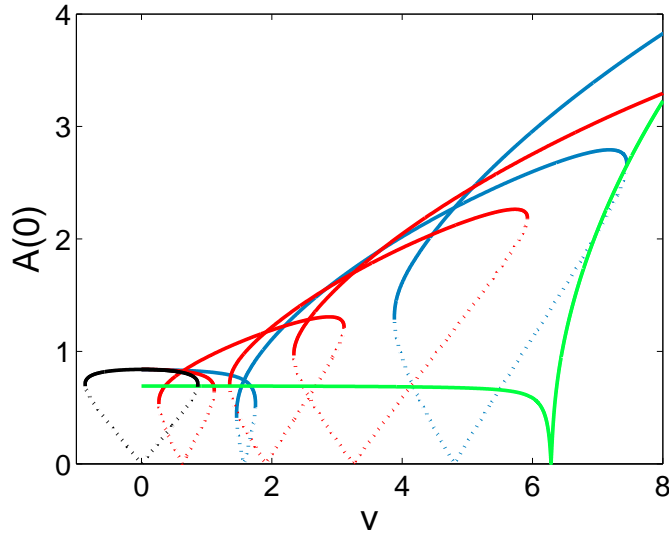


Figure 2. (Colour online) Connection between ring systems with finite lengths L (coloured) and the infinite domain (black line). We plot $A(0) = |u(0)|^2$ as a function of v for $\alpha = 0.5$ for several values of L , i.e. ∞ (black), 5 (red), 2 (blue), $1/2$ (green). Solid and dotted curves represent stable and unstable solutions, respectively.

center bifurcation between a dark soliton pinned to the obstacle and the uniform solution that is modified due to the inhomogeneity $U(x)$ [14]. The continuation diagram of the solution in this case forms a loop with its symmetric counterpart (note that Eq. (4) is invariant under the transformation $v \rightarrow -v$ and $x \rightarrow -x$) shown as black curve in Fig. 2. As v varies further, one will go around in the closed loop.

In a ring system, when L is finite, we do not obtain a closed loop, but have connected ‘loops’ instead. The situation, when the curves touch the horizontal axis for finite L , corresponds to the creation of dark-soliton-like states at the position of the impurity. Exactly at these points the topological charge increases. While in the infinite domain there is only one velocity point, where dark soliton-like-states can be created by the impurity, there are several of these points in the ring systems. The implications of this feature lead to complex dynamics as will be discussed further below.

With decreasing length L the initial ‘loops’ become smaller and the distance between two consecutive ‘loops’ increases. There will be critical values of L when the shrinking ‘loops’ become points, i.e. pairs of saddle-node bifurcations collide. In that case, when one decreases the length further, the corresponding ‘loops’ will disappear as is the case in the green curve in figure 2.

We have also studied the effect of varying the potential strength α on the existence of steady state solutions. From our computations shown in figure 3, we obtain that as α increases, the bifurcation ‘loops’ are getting smaller and two consecutive saddle-center bifurcation points get closer to each other and then finally disappear at some value α . This implies that there is a critical potential strength parameter α_{cr} above which there is no saddle-node bifurcation, i.e. the obstacle can move with any velocity without

breaking the superfluidity. This may be interpreted as a condition when the obstacle is strong enough to pin the ring BEC such that moving the obstacle means moving the BEC as a whole and hence there is no relative velocity between the two. The green curve ($L = 1/2$) in figure 2 also corresponds to such a situation. This is a feature that is not present in the infinite domain.

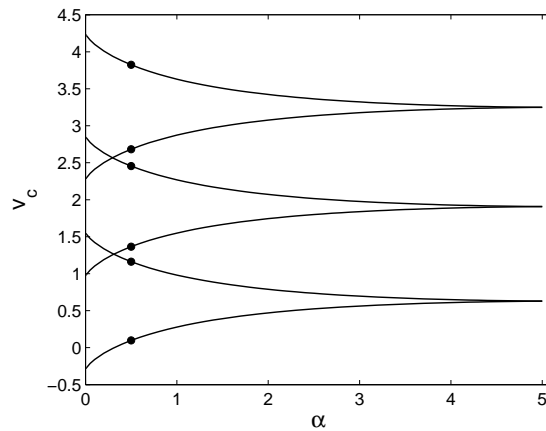


Figure 3. The critical velocities v_c as functions of the potential strength α , in a ring with $L = 5$. The black dots correspond to those depicted in figure 1. Above a certain critical strength the potential can move with any velocity without breaking the superfluidity. This is because the critical points pairwise merge, as shown in the figure. This is done in a way reminiscent of a swallowtail catastrophe surface [42] in the context of Fig. 1 and results in a monotonic dependence of the chemical potential μ vs. the velocity v and the absence of critical points.

The bifurcation diagrams can be analysed as follows. Using the Madelung’s transformation $u(x) = A(x)e^{i\varphi(x)}$, one obtains from the static version of (4)

$$A\varphi_{xx} = vA_x - 2A_x\varphi_x, \quad (6)$$

$$A_{xx} = A\varphi_x^2 - \mu A + A^3 - vA\varphi_x + U(x)A. \quad (7)$$

Multiplying (6) with A and integrating yields

$$\varphi_x = \frac{v}{2} - \frac{C_1}{A^2}, \quad (8)$$

where C_1 is a constant of integration, which can be directly taken to be any number in the infinite domain [14]. Notice that Eq. (8) is suggestive (as discussed above in connection with Fig. 2) of the fact that where $A(0) \rightarrow 0$, sharp gradients in the phase may arise; cf. the top profiles in Fig. 1. For a δ -potential $U(x)$, one then obtains from (7) the first integral

$$A_x^2 = \frac{1}{4A^2} [2A^6 - (4\mu + v^2)A^4 + 4C_2A^2 - 4C_1^2], \quad (9)$$

with C_2 being a constant of integration, and boundary conditions

$$A(0^+) = A(0^-), \quad A_x(0^+) - A_x(0^-) = \alpha A(0). \quad (10)$$

Due to the symmetry ($x \rightarrow -x$), the latter equation is equivalent to $A_x(0^+) = \alpha A(0)/2$. Using the equations in (3), which are equivalent to $A(-L) = A(L)$, $A_x(\pm L) = 0$, and (10), it is straightforward to obtain from (9) evaluated at $x = 0, L$ that

$$C_1^2 = \frac{(A(L)A(0))^2}{4} \left[4\mu + v^2 - 2(A(0)^2 + A(L)^2) + \frac{(\alpha A(0))^2}{A(0)^2 - A(L)^2} \right], \quad (11)$$

$$C_2 = \frac{1}{4} \left[2(A(0)^4 + A(L)^4) - (4\mu + v^2)(A(0)^2 + A(L)^2) - \frac{(\alpha A(0)^2)^2}{A(0)^2 - A(L)^2} \right]. \quad (12)$$

Let

$$Y(y) = \int \frac{dy}{\sqrt{2y^3 - (4\mu + v^2)y^2 + 4C_2y - 4C_1^2}}, \quad (13)$$

which can be expressed in terms of the incomplete elliptic integral of the first kind [43]. Then, the solution of (9) is

$$A(x) = \sqrt{Y^{-1}(x + Y(A(0)^2))}, \quad x > 0, \quad (14)$$

and $A(-x) = A(x)$. Hence, $A(L)$ can be written in terms of $A(0)$. Finally, using (8), one obtains the nonlinear algebraic equation that will yield the diagrams in Fig. 2, i.e.

$$\frac{vL}{2} - q\pi = \int_0^L \frac{C_1}{Y^{-1}(x + Y(A(0)^2))} dx, \quad (15)$$

where $q \in \mathbb{Z}$ is the topological charge. Figure 1 can be obtained similarly from solving (15) simultaneously with the constraint $\int_0^L Y^{-1}(x + Y(A(0)^2)) dx = N/2$ for μ and $A(0)$.

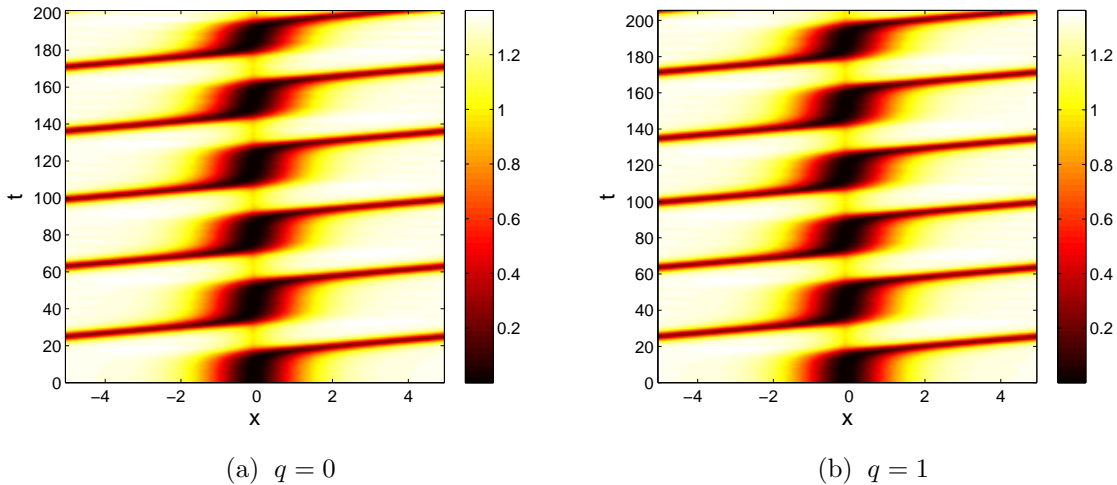


Figure 4. (Colour online) Time dynamics of the two unstable solutions shown in the insets of figure 1 for $q = 0$ and $v = 0.6$ (a) and $q = 1$ and $v = 1.9$ (b). In both panels, a soliton is created and moves around the ring with constant velocity, while the density of the BEC shows a periodic pattern.

It is then interesting to investigate the dynamics of solutions of eq. (4) in two specific regions of the bifurcation diagram. To be more precise, we study the time-evolution of unstable solutions under small perturbations (Figure 4) and discuss the time dynamics of solutions for velocities beyond the critical values (Figure 6), i.e. below or above which the corresponding steady state solutions do not exist.

For the two unstable solutions depicted in the insets of Figure 1, we show the time evolution dynamics in Figure 4 by plotting the density distribution along the ring. In both situations a dark soliton is released from the inhomogeneity at position $x = 0$ (black line) and travels at constant velocity around the ring. In figure 4(a), which corresponds to $q = 0$, the density of the cloud shows periodic fluctuations on long time scales, while in figure 4(b) where $q = 1$ the density fluctuations have a much shorter period.

We then analyse the dynamics beyond a critical value, i.e. we take the steady state solution at a critical velocity v_c as the initial condition and then compute the evolution for $v = v_c + \Delta v$.

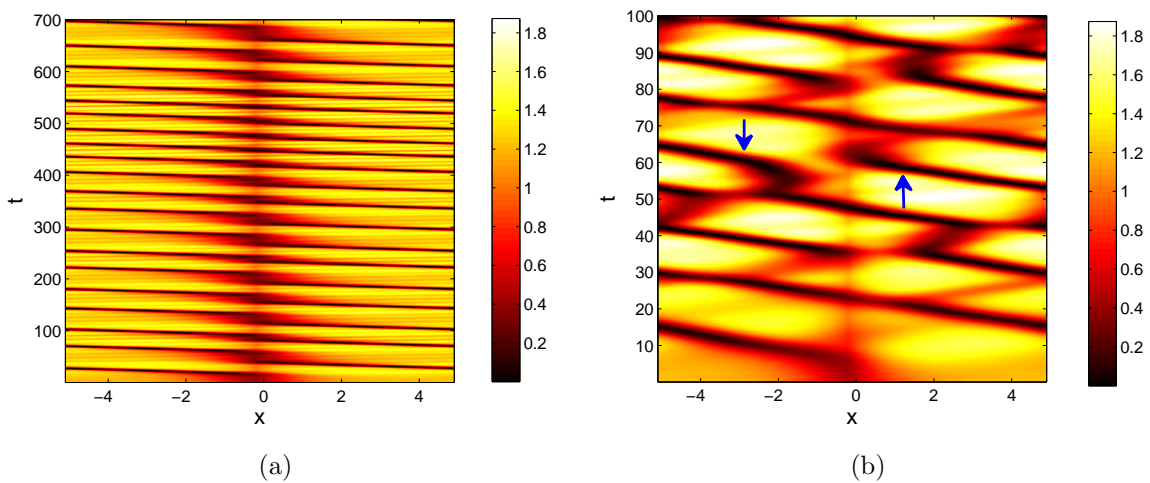


Figure 5. (Colour online) Numerical integration of eq. (4) at $v = 1.2 + \Delta v$ close to the bifurcation point. (a) For $\Delta v = 0.02$ a soliton is created at the position of the impurity, after one round-trip the soliton is trapped by the impurity and released after some time. (b) For $\Delta v = 0.6$ there are one or two solitons within the trap. Arrows in the figure indicate the presence of two solitons at one instant of time. See text for details.

In figure 5(a) we show the dynamics for $v = v_c + 0.02$ for the second bifurcation point in Figure 1 at $v_c = 1.2$. We observe that a dark soliton is emitted from the impurity along the evolution. In striking difference to the infinite domain [14], the released dark soliton interacts periodically with the impurity, which then traps the soliton for some time (e.g. between $t = 40$ and $t = 50$) before releasing it again. Note that the trapping time after each round trip is not constant. For a wide interval of $\Delta v > 0$ ($1.2 < v < 1.3$) we obtain similar dynamics with only one soliton present in the annular BEC. In the “laboratory frame” (where the obstacle is rotating), this situation implies that the emitted dark

soliton will tend to be standing, even though it also slowly drifts due to the temporary entrapment that it suffers from the moving obstacle.

When $\Delta v = 0.6$, one or two dark solitons can be created within the ring, as is shown in figure 5(b). For the first few time units, there is only one soliton present within the ring. After some time an additional dark soliton can be created, and as a result at the time instant indicated with arrows, two solitons exist in the trap. The presence of several solitons in the trap and repeated interaction with the impurity can lead to complex dynamics including collisions between the solitons or annihilation of the soliton by the impurity.

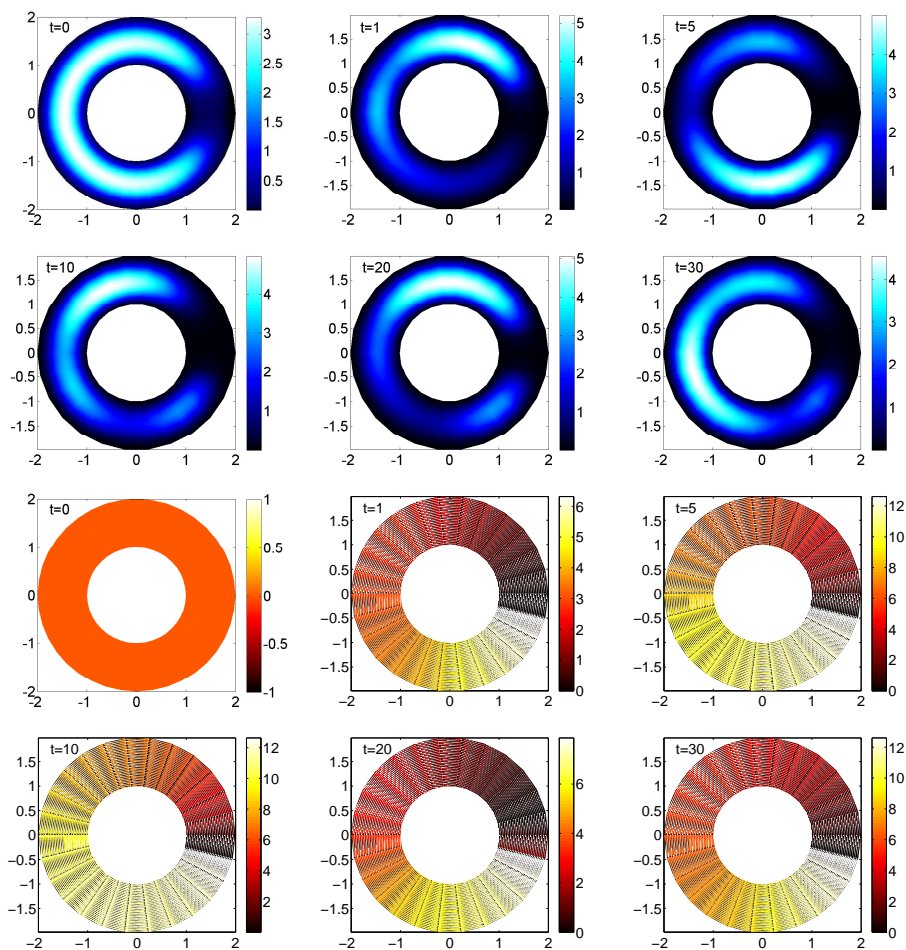


Figure 6. (Colour online) Numerical integration of Eq. (1) for a 2D ring in a rotating coordinate frame. The upper two rows show the population density at the indicated time, while the lower two rows are the corresponding phase distribution. Details of parameter values are in the text.

In addition to the 1D case we have also considered the quasi-two dimensional situation in (1) for superfluid states, i.e. static solutions. We obtain similar results as in 1D including the presence of critical currents and the production of one or several excitations when an obstacle moves with a velocity above a critical value.

Using $2R_i = R_o = 2$, $\alpha = 10$, $v = 3$ and $\mu = 11$, we visualize the dynamics above the critical point for the formation of persistent current in Figure 6 in a rotating coordinate frame. The initial condition was obtained from the steady state solution of Eq. (1) for $v \approx 0$. The velocity in Figure 6 is chosen such that the generation of phase slips associated with the release of localized modes can be seen almost immediately. The resulting density features a dip between two fractions of BECs moving clockwise from below and towards the obstacle. Observing the long-time dynamics of the integration, we also note that the number of 2π phase slips contained in the ring is limited, i.e., for the chosen parameter values it is either one or two. When, e.g., $t = 5, 10, 30$, one can note from the plot of the phase that there exists a double 2π phase winding, while there is only a single such winding when $t = 1, 20$.

4. Discussion and Future Challenges

In current state of the art ring traps that have been created e.g. by a spatial light modulator (SLM) [8] or by magnetic potentials [44], the impurity can easily be added through a focused blue detuned laser beam or by the SLM as well. In the setup of [7, 30] the impurity is present and excitations have indeed been observed [28]. The predictions of this paper are therefore directly relevant for the effects observed in current experiments.

In summary, we have studied the creation of dark solitary waves (and more generally the generation of phase slips/persistent currents) in a system with periodic boundary conditions. In contrast to the infinite domain case, for our bounded domain setting we find the existence of several critical velocities corresponding to different charges q of the stable solution. A somewhat unexpected feature was also the existence of sufficiently narrow domains or sufficiently strong obstacles for which no critical velocity could be identified. The ability to create coherent structures by increasing the velocity or to annihilate them through the impurity allows the creation –via the bifurcation diagram presented herein– of a controllable number of 2π phase windings within the ring trap. The analytical tractability of this formation through the quasi-1d theoretical formulation proposed herein is a feature adding to the controllability of the process. The exact dynamics of the resulting structures can be highly complex including possible collisions and interactions and will be an interesting object for further study. It is especially relevant to systematically extend such considerations to higher dimensional contexts not only in 2d but also in 3d.

HS, MS, APM and LH acknowledge the University of Nottingham for financial support through an EPSRC Bridging the Gaps grant. APM acknowledges CONACYT, this project was supported by EPSRC grant EP/K023624/1 and by the European Commission grant QuILMI - Quantum Integrated Light Matter Interface (No 295293). PK and IL also acknowledge EPSRC (EP/I017828/1) and EU (FET Proactive grant 601180 Matter- Wave). P.G.K. gratefully acknowledges the support of NSF-DMS-1312856, as well as from the BSF under grant 2010239, and the ERC under FP7, Marie Curie

Actions, People, International Research Staff Exchange Scheme (IRSES-605096).

References

- [1] Sauer J A, Barrett M D and Chapman M S 2001 *Phys. Rev. Lett.* **87** 270401.
- [2] Gupta S, Murch K W, Moore K L, Purdy T P, and Stamper-Kurn D M 2005 *Phys. Rev. Lett.* **95** 143201.
- [3] Arnold A S, Garvie C S, and Riis E 2006 *Phys. Rev. A* **73** 041606.
- [4] Henderson K, Ryu C, MacCormick C, and Boshier M G 2009 *New J. Phys.* **11** 043030.
- [5] Law K J H, Neely T W, Kevrekidis P G, Anderson B P, Bradley A S, Carretero-González R, 2014 *Phys. Rev. A* **89**, 053606.
- [6] Ryu C, Andersen M F, Clad P, Natarajan V, Helmerson K, and Phillips W D 2007 *Phys. Rev. Lett.* **99** 260401.
- [7] Ramanathan A, Wright K C, Muniz S R, Zelan M, Hill W T, Lobb C J, Helmerson K, Phillips W D, and Campbell G K 2011 *Phys. Rev. Lett.* **106** 130401.
- [8] Moulder S, Beattie S, Smith R P, Tammuz N, and Hadzibabic Z 2012 *Phys. Rev. A* **86** 013629.
- [9] Heathcote W H, Nugent E, Sheard B T, and Foot C J 2008 *New J. Phys.* **10** 043012.
- [10] Sherlock B E, Gildemeister M, Owen E, Nugent E, and Foot C J 2011 *Phys. Rev. A* **83** 043408.
- [11] Gustavson T L, Bouyer P, and Kasevich M A 1997 *Phys. Rev. Lett.* **78** 2046.
- [12] Raman C, Köhl M, Onofrio R, Durfee D S, Kukulewicz C E, Hadzibabic Z, and Ketterle W 1999 *Phys. Rev. Lett.* **83** 2502–2505.
- [13] Onofrio R, Raman C, Vogels J M, Abo-Shaeer J R, Chikkatur A P, and Ketterle W 2000 *Phys. Rev. Lett.* **85** 2228–2231.
- [14] Hakim V 1997 *Phys. Rev. E* **55** 2835.
- [15] Radouani A 2004 *Phys. Rev. A* **70** 013602.
- [16] Engels P and Atherton C 2007 *Phys. Rev. Lett.* **99** 160405.
- [17] Frisch T, Pomeau Y and Rica S 1992 *Phys. Rev. Lett.* **69** 1644; Jackson B, McCann J F, and Adams C S 1998 *Phys. Rev. Lett.* **80** 3903; Winiecki T, McCann J F and Adams C S 1999 *Phys. Rev. Lett.* **82** 5186.
- [18] Carusotto I, Hu S X, Collins L A, and Smerzi A 2006 *Phys. Rev. Lett.* **97** 260403.
- [19] Gladush Y G, El G A, Gammal A, and Kamchatnov A M 2007 *Phys. Rev. A* **75** 033619.
- [20] El G A, Gammal A, and Kamchatnov A M 2006 *Phys. Rev. Lett.* **97** 180405.
- [21] Luo C, Ibanescu M, Johnson S G and Joannopoulos J D 2003 *Science* **299** 368.
- [22] Neely T W, Samson E C, Bradley A S, Davis M J, Anderson B P 2010 *Phys. Rev. Lett.* **104** 160401.
- [23] Pavloff N *Phys. Rev. A* 2002 **66** 013610.
- [24] Dubessy R, Liennard T, Pedri P, and Perrin H 2012 *Phys. Rev. A* **86** 011602(R).
- [25] Fedichev P O and Shlyapnikov G V 2001 *Phys. Rev. A* **63** 045601.
- [26] Anglin J R 2001 *Phys. Rev. Lett.* **87** 240401.
- [27] Piazza F, Collins L A, and Smerzi A 2009 *Phys. Rev. A* **80** 021601(R).
- [28] Wright K C, Blakestad R B, Lobb C J, Phillips W D, and Campbell G K 2013 *Phys. Rev. Lett.* **110** 025302.
- [29] Eckel S, Lee J G, Jendrecejewski F, Murray N, Clark C W, Lobb C J, Phillips W D, Edwards M and Campbell C K 2014 *Nature* **506**, 200.
- [30] Ryu C, Blackburn P W, Blinova A A and Boshier M G 2013 *Phys. Rev. Lett.* **111** 205301.
- [31] Jendrecejewski F, Eckel S, Murray N, Lanier C, Edwards M, Lobb C J, Campbell C K 2014 *Phys. Rev. Lett.* **113** 045305.
- [32] Mathey A C, Clark C W and Mathey L 2014 *Phys. Rev. A* **90**, 023604.
- [33] Piazza F, Collins L A, and Smerzi A 2013 *J. Phys. B: At. Mol. Opt. Phys.* **46** 095302.
- [34] Kanamoto R, Carr L D and Ueda M 2008 *Phys. Rev. Lett.* **100** 060401.
- [35] Kanamoto R, Carr L D and Ueda M 2009 *Phys. Rev. A* **79** 063616.

- [36] Kanamoto R, Carr L D and Ueda M 2010 *Phys. Rev. A* **81** 023625.
- [37] Eckel S, Jendrecejewski F, Kumar A, Lobb C J, Campbell C K 2014 *Phys. Rev. X* **4** 031052.
- [38] Cominotti M, Rossini D, Rizzi M, Hekking F and Minguzzi A 2014 *Phys. Rev. Lett.* **113** 025301.
- [39] Carr L.D., Leung M.A., and Reinhardt W.P. 2000 *J. Phys. B: At. Mol. Opt. Phys.* **33** 3983.
- [40] Parker N 2004 *Numerical Studies of Vortices and Dark Solitons in Atomic Bose-Einstein Condensates* (PhD Thesis) University of Durham.
- [41] R. Seydel, *Practical Bifurcation and Stability Analysis* (Springer-Verlag, New York, 2010).
- [42] See e.g. the relevant discussion of this catastrophe in: https://en.wikipedia.org/wiki/Catastrophe_theory
- [43] Olver F W J, Lozier D W, Boisvert R F, and Clark C W (Eds.), *NIST Handbook of Mathematical Functions* (Cambridge University Press, Cambridge, 2010).
- [44] Pritchard J D, Dinkelaker A N, Arnold A S, Griffin P F and Riis E 2012 *New J. Phys.* **14** 103047.